
SELECTIVE HYDROGENATION PROMOTES ANISOTROPIC THERMOELECTRIC PROPERTIES OF TPDH-GRAPHENE

Caique Campos de Oliveira

Center for Natural and Human Sciences (CCNH)
Federal University of ABC (UFABC)
Santo André - SP, 09210-170, Brazil.
caique.campos@aluno.ufabc.edu.br

Douglas Soares Galvao

Physics Institute Gleb Wataghin (IFGW)
State University of Campinas (UNICAMP)
Campinas/SP, Brazil
galvao@ifi.unicamp.br

Pedro Alves da Silva Autreto

Center for Natural and Human Sciences (CCNH)
Federal University of ABC (UFABC)
Santo André - SP, 09210-170, Brazil.
pedro.autreto@ufabc.edu.br

ABSTRACT

We have combined DFT calculations with the Boltzmann semiclassical transport theory to investigate the effect of selective hydrogenation on the thermoelectric properties of tetra-penta-deca-hexagonal graphene (TPDH-gr), a recently proposed new 2D carbon allotrope. Our results show that the Seebeck coefficient is enhanced after hydrogenation. The conductivity along the x direction is increased almost eight times while being almost suppressed along the y direction. This behavior can be understood in terms of the electronic structure changes due to the appearance of a Dirac-like cone after the selective hydrogenation. Consistent with the literature, the electronic contribution to thermal conductivity displays the same qualitative behavior as the conductivity, as expected from the Wiedemann-Franz law. The increase in thermal conductivity with temperature limits the material's power factor. The significant increase in the Seebeck coefficient and conductivity increases also contribute to the thermal conductivity increase. These results show that hydrogenation is an effective method to improve the TPDH-gr thermoelectric properties, and this carbon allotrope can be an effective material for thermoelectric applications.

1 Introduction

Anisotropic physical properties generally originate from structural low symmetry [1]. Orthorhombic, monoclinic, and triclinic lattices are likely to exhibit directional-dependent properties due to the non-symmetrical chemical environment of the atoms in these structures [2]. Examples of such materials include low-symmetry chalcogenides like ReX_2 ($X = \text{S}$ or Se) with anisotropic optical properties [3], materials with non-trivial electronic topology (e.g., Weyl-semimetals, such as $\text{Nb}(\text{S}, \text{As})$) [4], and bismuth tellurides [5]. Metal-free materials can also exhibit anisotropy. In black phosphorus (BP), the different hybridization of each P atom results in anisotropic electrical properties [6]. Borophenes, 2D boron monolayers [7, 8] exhibit anisotropic mechanical [9] and thermal [10] properties.

Directional-dependent properties are highly desirable in some energy harvesting applications, including thermal energy recycling through Seebeck or Peltier effects [11–13]. The rise of two-dimensional (2D) compounds opened new perspectives in the development of next-generation nanodevices. In contrast to 3D or “bulk” materials, their 2D counterparts exhibit reduced thickness with a large surface-to-volume ratio, giving rise to electronic confinement effects that can be engineered to tune structural, electronic, optical, and thermoelectric properties [2, 14]. 2D carbon allotropes represent an exciting group of these materials due to their unique structural and electronic properties. The hybridization of valence orbitals in carbon enables the existence of topologically different allotropes, such as graphene [15], graphynes [16, 17], biphenylenes [18], among others.

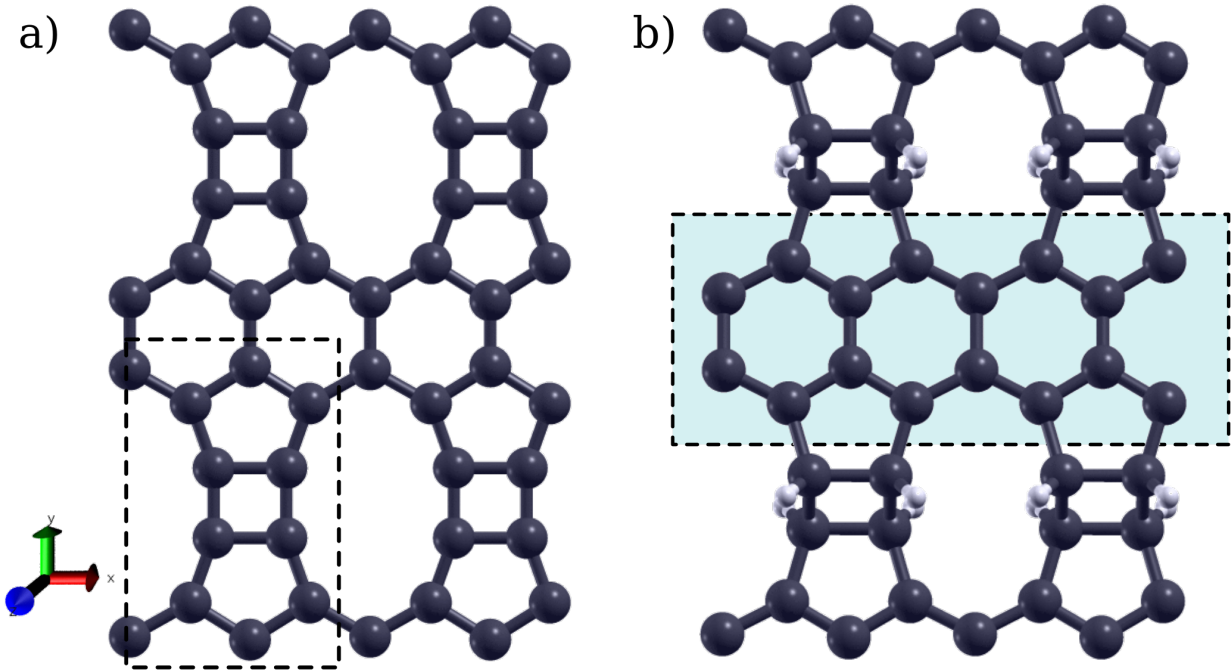


Figure 1: a) A 2x2 TPDH-gr supercell. b) a 2x2 hTPDH-gr. The hexagonal carbon rings along the x direction are highlighted in the dashed light green rectangle.

From an environmental perspective, carbon-based materials are attractive due to their high availability, non-toxicity, and eco-friendliness [13]. Their physical properties are also technologically attractive. Graphene, for example, exhibits excellent mechanical, optical, electrical, and thermal properties suitable for electronics, optoelectronics, and sensing [19]. However, its gapless electronic behavior and exceptionally high thermal conductance hinder its thermoelectric applications [20, 21]. The enhancement of thermoelectric properties of materials requires the modulation of electrical and thermal conduction [22] and can be achieved by nanostructuring, doping/defects [20] and functionalization [23, 24].

Recently, novel carbon 2D allotropes have been experimentally realized, such as graphynes [16, 17] and biphenylenes [18]. Biphenylenes are of particular interest because they combine different carbon rings that can lead to low-symmetry anisotropic systems. Tetra-penta-deca-hexagonal graphene (TPDH-gr, Figure 1(a)) is another example of such structures. TPDH-gr exhibits in-plane elastic anisotropy and significant optical adsorption in short wavelength range, making it promising as a coating material for UV protection [25]. However, TPDH-gr presents semimetallic behavior, which is known to limit thermoelectric performance. Fortunately, this limitation can be overcome by attaching hydrogen adatoms to the structures to tune the electronic properties. This methodology has been successfully applied to other 2D metal-free structures, including carbon, silicon, and germanium-like ones [26, 27].

We have recently shown that the hydrogenation of TPDH-gr occurs mainly at the tetragonal rings, producing transversal lines of hydrogen atoms with non-hydrogenated hexagon rings along the x-direction, as highlighted in Figure 1(b). These structural changes result in electronic changes, giving rise to Dirac's cone features [28]. However, this study was limited to investigating the structural and electronic changes. In this work, we applied first-principles calculations (Density Functional Theory (DFT)) together with the Boltzmann semiclassical transport equation to investigate the effects of hydrogenation on the transport properties of pristine and hydrogenated TPDH-gr. We also applied the Boltzmann transport theory to calculate the thermoelectric properties of pristine and hydrogenated TPDH-gr. Our results show that both structures present significant anisotropic behavior, and selective hydrogenation enhances this behavior by almost suppressing the electrical conduction along particular directions.

2 Computational Methods

First-principles calculations were carried out using density functional theory as implemented in the Quantum ESPRESSO package [29]. Core electrons were approximated by the pseudopotentials (pp) method, using the solid standard state (SSSP) library [30]. Kohn-sham orbitals were expanded using a plane wave basis set imposing a threshold of 60 Ry

for the kinetic energy and a 480 Ry one for the electronic density, as suggested by the pp efficiency set of SSSP. The Brillouin zone was sampled by a $(16 \times 16 \times 1) 6 \times 6 \times 1$ k-point mesh for (non)self-consistent calculations following the Monkhorst-Pack scheme [31]. The threshold for self-consistency of electronic density was set to 10^{-7} Ry, while the energy and forces between two consecutive ionic steps were minimized until 10^{-4} Ry and 10^{-3} Ry/Bohr, respectively. The exchange and correlation interactions were approximated by the generalized gradient parametrized by Perdew, Burke, and Ernzerhoff (GGA-PBE) [32].

The electronic transport coefficients were calculated using Boltzmann semiclassical transport equations within the relaxation time approximation. The conductivity (σ), Seebeck coefficient (S), and electrical contribution to thermal conductivity (κ_e) tensors were obtained from analytical expressions as functions of temperature (T) and chemical potential (μ) using the transport kernel ($\Xi_{ij}(\epsilon)$):

$$\sigma_{ij}(T, \mu) = \frac{1}{\Omega} \int \Xi_{ij}(\epsilon) \left[\frac{-\partial f_{\mu}(T, \epsilon)}{\partial \epsilon} \right] d\epsilon \quad (1)$$

$$(\kappa_e)_{ij}(T, \mu) = \frac{1}{e^2 T \Omega} \int \Xi_{ij}(\epsilon - \mu)^2 \left[\frac{-\partial f_{\mu}(T, \epsilon)}{\partial \epsilon} \right] d\epsilon \quad (2)$$

$$S_{ij} = \frac{1}{e T \Omega \sigma_{ij}} \int \Xi_{ij}(\epsilon - \mu) \left[\frac{-\partial f_{\mu}(T, \epsilon)}{\partial \epsilon} \right] d\epsilon \quad (3)$$

Where e is the electrical charge, Ω is the cell total volume, ϵ is the electronic band energy, and $f_{\mu}(T, \epsilon)$ is the carrier distribution function. The i and j indexes represent the cartesian components. BoltzTraP code [33] performs a Fourier expansion of the band energies, interpolating these values to obtain an analytical function that is used to evaluate the thermoelectric coefficients S , σ/τ , and κ_e/τ , where τ is the time relaxation parameter. These coefficients are calculated within the rigid band approximation, assuming that the band structure does not significantly change for different doping levels [24, 33, 34].

3 Results and Discussion

3.1 Seebeck Coefficient

The conversion of waste heat into electricity can be achieved by exploiting the Seebeck or Peltier effects. The Seebeck coefficient (S) represents the maximum potential difference created in the material when a temperature gradient is present [13]. The x and y components of the S tensor for pristine and hydrogenated TPDH-gr are presented in Figure 2. Pristine TPDH-gr displays a small S coefficient around the Fermi level for both directions. This is typical for metals due to the symmetry of electrons and holes caused by the absence of an electronic band gap [35]. Also, as the temperature increases, the profile of the curves becomes very similar, indicating that the Seebeck coefficient reaches a peak value. Analyzing the S tensor as a function of the temperature (T) (Fig S.1), it is possible to infer that the x component of S for pristine TPDH-gr is zero for $T = 700$ K, while the y -component reaches a limit value of $\sim 80 \mu\text{V/K}$ at $T = 500$ K. The corresponding curves for hydrogenated TPDH-gr are also different for the x and y directions, as expected from the material structural anisotropy. When the structure is hydrogenated, the Seebeck coefficient exhibits a peak near the Fermi level, reaching $200 \mu\text{V/K}$ at 300 K for both directions. The inverse sign of the peaks indicates that the charge carriers are holes (for the positive peak) and electrons (for the negative one) [34]. For both analyzed directions, the peaks' amplitude decreases with increasing temperature, although this behavior is more pronounced for the y direction, showing that the anisotropic behavior is preserved. The decrease can be attributed to the increase in thermal energy, similar to the observed in other materials [36].

3.2 Electric and Electronic contribution to Thermal Conduction

In Figure 3, we present the results for the electrical and thermal conductivities as a function of temperature for the pristine and hydrogenated TPDH-gr. From Figure 3, the anisotropic behavior is evident. The conductivity along the x direction is constant (roughly $1 \times 10^{19} (\Omega.m.s)^{-1}$). In contrast, the y component increases with temperature: for $T = 300\text{K}$, $\sigma_y \approx 3 \times 10^{19} (\Omega.m.s)^{-1}$ reaching $\sigma_y = 4.5 \times 10^{19} (\Omega.m.s)^{-1}$ for $T > 700$ K. A similar behavior is observed for the thermal conductivity.

These results can be explained in terms of the electronic structure (presented in Fig. S.2). Pristine TPDH-gr exhibits an electronic band structure with the valence band crossing the Fermi energy level along the $\Gamma \rightarrow Y$ (Figure 4(b)). From the Brillouin zone of the orthorhombic cell (see Figure 4), it becomes clear that this path is directly related to the y direction. After hydrogenation, this behavior changes completely. The conductivity is almost eight times higher along

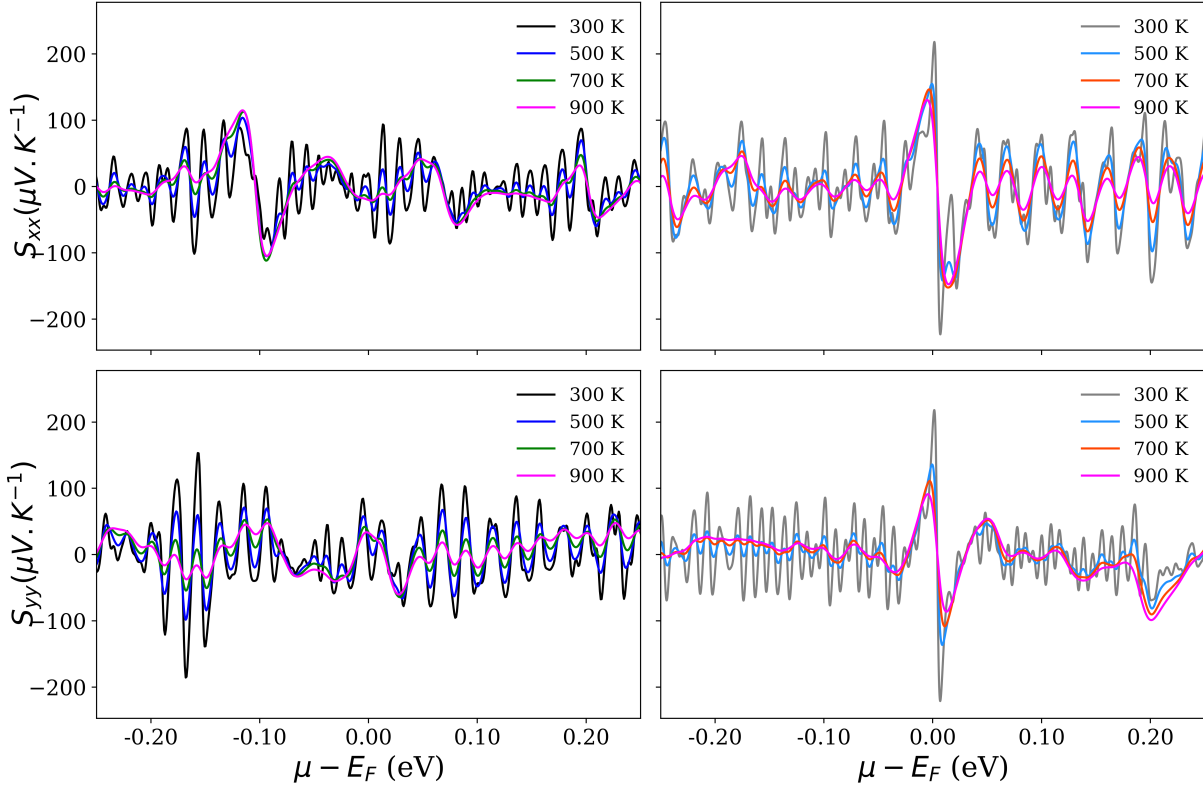


Figure 2: a) Seebeck coefficient as a function of the chemical potential (μ) shifted relative to the Fermi energy tensor components for the x (top) and y (bottom) directions, for pristine (left) and hydrogenated (right) TPDH-gr at different temperature.

the x direction compared to the pristine structure, ranging from $\sigma_x = 7.0 \times 10^{19}$ ($T = 300$ K) to $\sigma_x = 8.0 \times 10^{19}$ ($\Omega.m.s$) $^{-1}$ at $T = 900$ K. σ_y is substantially reduced, exhibiting an almost constant value of 0.5×10^{19} ($\Omega.m.s$) $^{-1}$. This results in a variation in the ratio of conductivities (σ_x/σ_y) ranging between 14 and 16 as the temperature rises.

We can understand these changes by analyzing the electronic structure of the hydrogenated system (Figure 4 and Fig. S2.b). We can see that there is a Dirac-type cone along the $\Gamma \rightarrow X$ path, while at the $\Gamma \rightarrow Y$ one, the structure displays only a small bandgap at the Y symmetry point. Also, these changes are consistent with the electronic structures of nanoribbons studied by Bathacharya and Jana [25]. The nanoribbons along the y direction (involving tetra and pentagonal rings) are semiconductors, while the nanoribbons along the x direction (involving pentagonal rings, see Figure 1(b)) are metallic. Topologically, we can consider that after hydrogenation, there is a confinement of the electrons through the homogeneous stripes composed of hexagonal rings (Figure 1(b)), which are expected to exhibit a higher conductivity when compared to the y direction (inhomogeneous ring arrays).

The results for the electronic contribution to the thermal conductivity (κ_e) show a temperature dependence for both components. An increase in thermal conductivity is expected due to increased thermal energy. The x direction also shows a lower conductivity when compared to the y direction. When the structure is hydrogenated, κ_{ex} increases while κ_{ey} drops substantially. This indicates that hydrogenation also promotes thermal transport along the x direction while suppressing the transversal heat conduction. These results are the opposite of the hydrogenation of graphene but agree with the results for penta-graphene, in which the enhancement in the thermal conductivity was attributed to weaker phonon scattering due to larger bond anharmonicity [23]. Both components display similar behavior relative to the electric conductivity (σ), an expected result since these quantities are related by the Wiedemann-Franz law [37]. The anisotropy of hydrogenated TPDH-gr could be useful in electronic applications in which directional electric currents are applied.

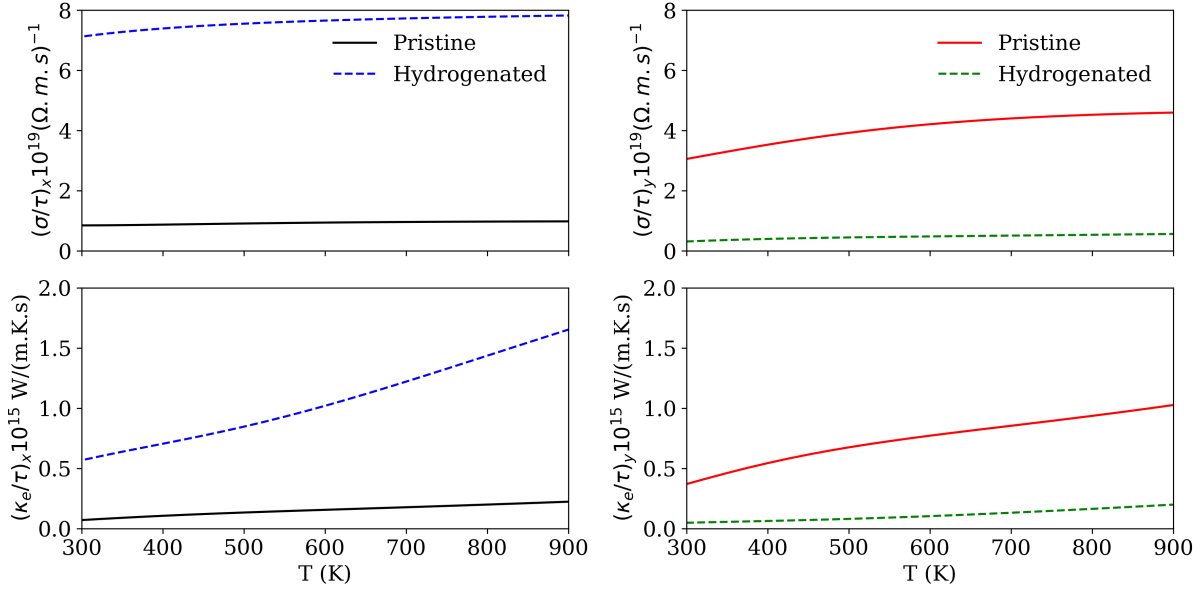


Figure 3: a) Electrical (top) and thermal (bottom) conductivity tensor components along the x (left) and y (right) directions for pristine (solid) and hydrogenated (dashed) TPDH-gr.

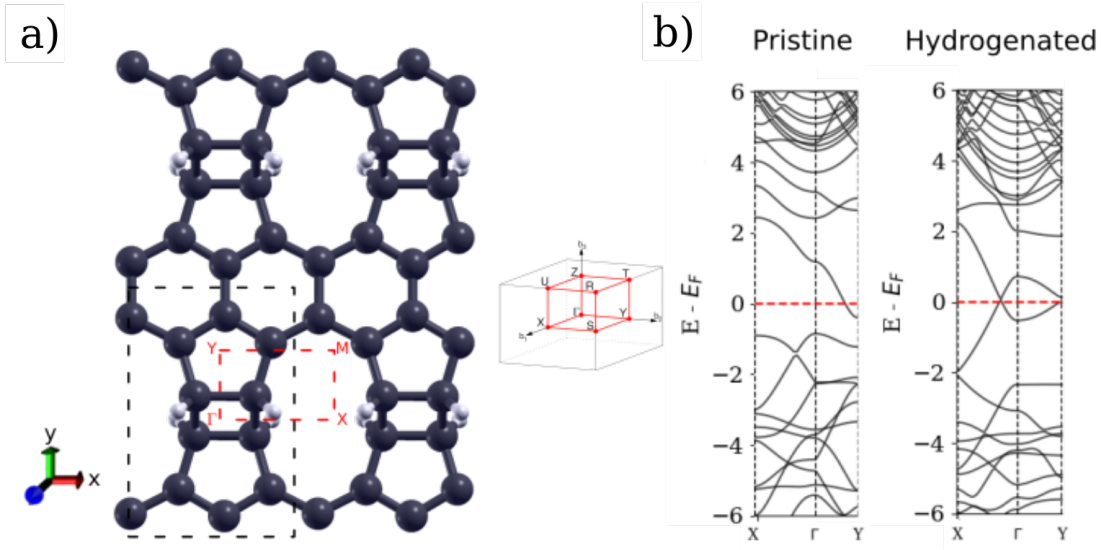


Figure 4: a) A hTPDH-gr 2x2 supercell. The black-dashed lines indicate the corresponding unit cell, while the red-dashed ones indicate the high-symmetry points (Γ , X, Y, and M) in the first Brillouin zone of the orthorhombic lattice system (inset). (b) Electronic band structure for pristine and hydrogenated TPDH-gr along the X → Γ → Y path high-symmetry points.

3.3 Power Factor

The thermoelectric conversion capacity, representing the maximum power available, can be expressed by the power factor (PF) given by the product $S^2\sigma$. The x and y components of the PF are presented in Figure 5.

As expected, pristine TPDH-gr presents a poor thermoelectric conversion capacity. It has an almost zero PF along the x direction and a maximum of $5x \times 10^{10} W/(mk^2s)$ along the y direction. For comparison, the PF of 6% compressed n-type doped hydrogenated germanene can reach $57.21 \times 10^{10} W/(mK^2s)$ at $T = 800 K$ [37]. The PF of Zintl phase (Sr,Ba)Ag₂SeTe compounds can reach $17.1 \times 10^{10} W/(mK^2s)$ at 300K reaching almost $70 \times 10^{10} W/(mKs)$

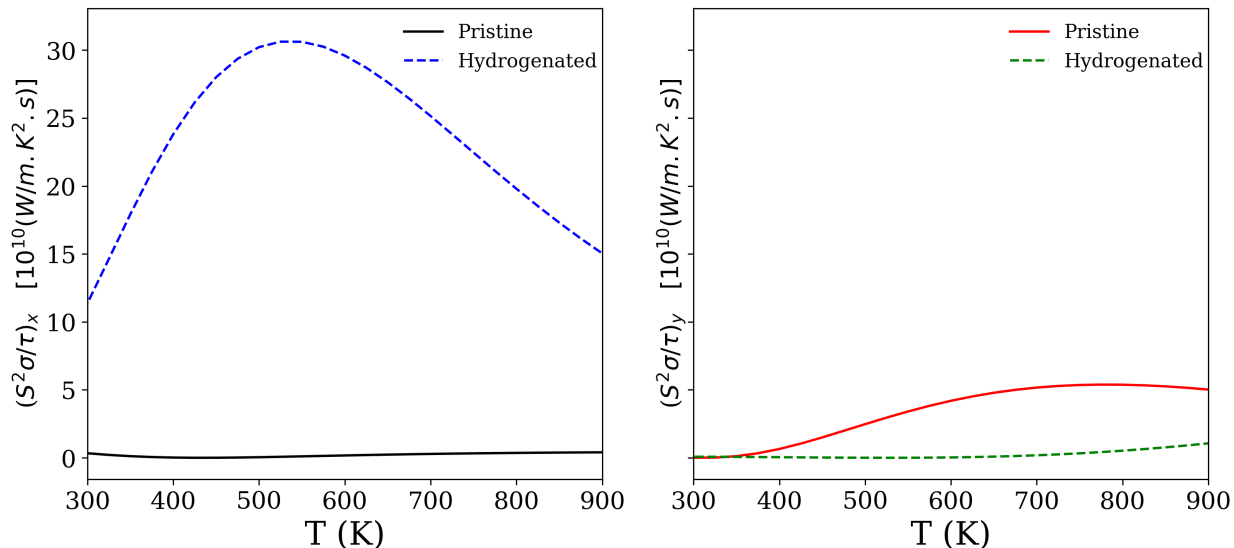


Figure 5: a) Power factor components for x and y directions. Solid and dashed curves refer to pristine and hydrogenated results, respectively.

at $T = 1200$ K [38]. After hydrogenation, the corresponding PF x-component is significantly enhanced, reaching $30 \times 10^{10} \text{ W/(mKs)}$ at $T \approx 530$ K, while the y component is almost suppressed (near zero PF value).

These results can be understood in terms of the changes in the electrical conductivity caused by hydrogenation. There are two main contributing factors to the thermoelectric properties of a material: the Seebeck coefficient and the lattice thermal conduction ($\kappa = \kappa_{ph} + \kappa_e$) [35]. While hydrogenation was shown to promote the thermoelectric conversion by increasing S , κ_e was also increased, as seen by the increase in the x component (Figure 3(c, d)). Therefore, to further improve the TPDH-gr thermoelectric properties, there are two directions to follow: (i) further enhancement of the Seebeck coefficient, which could be achieved by increasing the hydrogen-carbon ratio, thus possibly increasing the electronic bandgap. (ii) decrease the thermal lattice conductivity by increasing phonon scattering. Combining these two strategies, enhancing the TPDH-gr figure of merit (ZT) should be possible.

4 Conclusions

In this work, we have combined DFT calculations with the Boltzmann semiclassical transport theory to investigate the effect of hydrogenation on the thermoelectric properties of TPDH-gr. Our results show that TPDH-gr thermoelectric properties are intrinsically anisotropic due to the low symmetry of the lattice system. Furthermore, the Seebeck coefficient is enhanced after hydrogenation due to the changes in the material's electronic structure after selective hydrogenation of the tetragonal rings. Interestingly, the conductivity along the x direction is increased almost eight times while being almost suppressed along the y direction. This behavior can be understood in terms of the electronic structure changes due to the appearance of a Dirac-like cone after the selective hydrogenation. Consistent with the literature, the electronic contribution to thermal conductivity displays the same qualitative behavior as the conductivity, as expected from the Wiedemann-Franz law. The increase of thermal conductivity with temperature limits the material's power factor. The significant increase in the Seebeck coefficient and conductivity increases also contribute to the thermal conductivity increase. These results show that hydrogenation is an effective method to improve the TPDH-gr thermoelectric properties, and this carbon allotrope can be an effective material for thermoelectric applications. Considering the recent advances in the synthesis of new 2D carbon allotropes [17, 18, 39], including structures with some of the same TPDH-gr carbon rings [18], the TPDH-gr synthesis can be considered feasible with our present-day synthesis capabilities.

Conflicts of interest

There are no conflicts to declare.

Acknowledgements

CCO thanks PRH.49 (PRH-ANP UFABC) for funding and UFABC Multiuser Computational Center (CCM-UFABC) for computational resources provided. DSG thanks the Center for Computational Engineering & Sciences (CCES) at Unicamp for financial support through the FAPESP/CEPID Grant 2013/08293-7 and PASA to CNPq (Grant 308428/2022-6).

References

- [1] S. Zhao, B. Dong, H. Wang, H. Wang, Y. Zhang, Z. V. Han, and H. Zhang, “In-plane anisotropic electronics based on low-symmetry 2d materials: progress and prospects,” *Nanoscale Adv.*, vol. 2, pp. 109–139, 2020.
- [2] J. Zhao, D. Ma, C. Wang, Z. Guo, B. Zhang, J. Li, G. Nie, N. Xie, and H. Zhang, “Recent advances in anisotropic two-dimensional materials and device applications,” *Nano Research*, vol. 14, pp. 897–919, Apr 2021.
- [3] J. P. Echeverry and I. C. Gerber, “Theoretical investigations of the anisotropic optical properties of distorted $1t$ res_2 and $rese_2$ monolayers, bilayers, and in the bulk limit,” *Phys. Rev. B*, vol. 97, p. 075123, Feb 2018.
- [4] Y. Zhou, Y.-Q. Zhao, Z.-Y. Zeng, X.-R. Chen, and H.-Y. Geng, “Anisotropic thermoelectric properties of weyl semimetal nbx ($x = p$ and as): a potential thermoelectric material,” *Phys. Chem. Chem. Phys.*, vol. 21, pp. 15167–15176, 2019.
- [5] I. T. Witting, T. C. Chasapis, F. Ricci, M. Peters, N. A. Heinz, G. Hautier, and G. J. Snyder, “The thermoelectric properties of bismuth telluride,” *Advanced Electronic Materials*, vol. 5, no. 6, p. 1800904, 2019.
- [6] F. Xia, H. Wang, and Y. Jia, “Rediscovering black phosphorus as an anisotropic layered material for optoelectronics and electronics,” *Nature Communications*, vol. 5, p. 4458, Jul 2014.
- [7] Z. A. Piazza, H.-S. Hu, W.-L. Li, Y.-F. Zhao, J. Li, and L.-S. Wang, “Planar hexagonal $b36$ as a potential basis for extended single-atom layer boron sheets,” *Nature Communications*, vol. 5, p. 3113, Jan 2014.
- [8] B. Feng, J. Zhang, Q. Zhong, W. Li, S. Li, H. Li, P. Cheng, S. Meng, L. Chen, and K. Wu, “Experimental realization of two-dimensional boron sheets,” *Nature Chemistry*, vol. 8, pp. 563–568, Jun 2016.
- [9] Z. Zhang, Y. Yang, E. S. Penev, and B. I. Yakobson, “Elasticity, flexibility, and ideal strength of borophenes,” *Advanced Functional Materials*, vol. 27, no. 9, p. 1605059, 2017.
- [10] H. Zhou, Y. Cai, G. Zhang, and Y.-W. Zhang, “Superior lattice thermal conductance of single-layer borophene,” *npj 2D Materials and Applications*, vol. 1, p. 14, Jun 2017.
- [11] A. T. Burkov, A. Heinrich, and M. V. Vedernikov, “Anisotropic thermoelectric materials, properties and applications,” *AIP Conference Proceedings*, vol. 316, pp. 76–80, 08 1994.
- [12] P. Chakraborty, T. Ma, A. H. Zehri, L. Cao, and Y. Wang, “Carbon-based materials for thermoelectrics,” *Advances in Condensed Matter Physics*, vol. 2018, p. 3898479, Jul 2018.
- [13] J.-S. Yun, S. Choi, and S. H. Im, “Advances in carbon-based thermoelectric materials for high-performance, flexible thermoelectric devices,” *Carbon Energy*, vol. 3, no. 5, pp. 667–708, 2021.
- [14] M. Dresselhaus, G. Chen, M. Tang, R. Yang, H. Lee, D. Wang, Z. Ren, J.-P. Fleurial, and P. Gogna, “New directions for low-dimensional thermoelectric materials,” *Advanced Materials*, vol. 19, no. 8, pp. 1043–1053, 2007.
- [15] K. S. Novoselov, A. K. Geim, S. V. Morozov, D. Jiang, Y. Zhang, S. V. Dubonos, I. V. Grigorieva, and A. A. Firsov, “Electric field effect in atomically thin carbon films,” *Science*, vol. 306, no. 5696, pp. 666–669, 2004.
- [16] A. Ivanovskii, “Graphynes and graphdynes,” *Progress in Solid State Chemistry*, vol. 41, no. 1, pp. 1–19, 2013.
- [17] V. G. Desyatkin, W. B. Martin, A. E. Aliev, N. E. Chapman, A. F. Fonseca, D. S. Galvão, E. R. Miller, K. H. Stone, Z. Wang, D. Zakhidov, F. T. Limpoco, S. R. Almahdali, S. M. Parker, R. H. Baughman, and V. O. Rodionov, “Scalable synthesis and characterization of multilayer γ -graphyne, new carbon crystals with a small direct band gap,” *Journal of the American Chemical Society*, vol. 144, pp. 17999–18008, Oct 2022.
- [18] Q. Fan, L. Yan, M. W. Tripp, O. Krejčí, S. Dimosthenous, S. R. Kachel, M. Chen, A. S. Foster, U. Koert, P. Liljeroth, and J. M. Gottfried, “Biphenylene network: A nonbenzenoid carbon allotrope,” *Science*, vol. 372, no. 6544, pp. 852–856, 2021.
- [19] M. Sang, J. Shin, K. Kim, and K. J. Yu, “Electronic and thermal properties of graphene and recent advances in graphene based electronics applications,” *Nanomaterials*, vol. 9, no. 3, 2019.

- [20] M. S. K. K. Tabitha A. Amollo, Genene T. Mola and V. O. Nyamori, “Graphene for thermoelectric applications: Prospects and challenges,” *Critical Reviews in Solid State and Materials Sciences*, vol. 43, no. 2, pp. 133–157, 2018.
- [21] P. Dollfus, V. H. Nguyen, and J. Saint-Martin, “Thermoelectric effects in graphene nanostructures,” *Journal of Physics: Condensed Matter*, vol. 27, p. 133204, mar 2015.
- [22] M. Wolf, R. Hinterding, and A. Feldhoff, “High power factor vs. high zT —a review of thermoelectric materials for high-temperature application,” *Entropy*, vol. 21, no. 11, 2019.
- [23] X. Wu, V. Varshney, J. Lee, T. Zhang, J. L. Wohlwend, A. K. Roy, and T. Luo, “Hydrogenation of penta-graphene leads to unexpected large improvement in thermal conductivity,” *Nano Letters*, vol. 16, pp. 3925–3935, Jun 2016.
- [24] Y. F. Li, G. H. Tang, and B. Fu, “Hydrogenation: An effective strategy to improve the thermoelectric properties of multilayer silicene,” *Phys. Rev. B*, vol. 99, p. 235428, Jun 2019.
- [25] D. Bhattacharya and D. Jana, “Tpdh-graphene: A new two dimensional metallic carbon with ndr behaviour of its one-dimensional derivatives,” *Physica E: Low-dimensional Systems and Nanostructures*, vol. 127, p. 114569, 2021.
- [26] H. Sahin, O. Leenaerts, S. K. Singh, and F. M. Peeters, “Graphane: From synthesis to applications,” 2015.
- [27] S. Trivedi, A. Srivastava, and R. Kurchania, “Silicene and germanene: A first principle study of electronic structure and effect of hydrogenation-passivation,” *Journal of Computational and Theoretical Nanoscience*, vol. 11, no. 3, pp. 781–788, 2014.
- [28] C. C. Oliveira, M. Medina, D. S. Galvao, and P. A. S. Autreto, “Tetra-penta-deca-hexagonal-graphene (tpdh-graphene) hydrogenation patterns: dynamics and electronic structure,” *Phys. Chem. Chem. Phys.*, vol. 25, pp. 13088–13093, 2023.
- [29] P. Giannozzi, O. Andreussi, T. Brumme, O. Bunau, M. B. Nardelli, M. Calandra, R. Car, C. Cavazzoni, D. Ceresoli, M. Cococcioni, N. Colonna, I. Carnimeo, A. D. Corso, S. de Gironcoli, P. Delugas, R. A. DiStasio, A. Ferretti, A. Floris, G. Fratesi, G. Fugallo, R. Gebauer, U. Gerstmann, F. Giustino, T. Gorni, J. Jia, M. Kawamura, H.-Y. Ko, A. Kokalj, E. Küçükbenli, M. Lazzeri, M. Marsili, N. Marzari, F. Mauri, N. L. Nguyen, H.-V. Nguyen, A. O. de-la Roza, L. Paulatto, S. Ponc , D. Rocca, R. Sabatini, B. Santra, M. Schlipf, A. P. Seitsonen, A. Smogunov, I. Timrov, T. Thonhauser, P. Umari, N. Vast, X. Wu, and S. Baroni, “Advanced capabilities for materials modelling with quantum espresso,” *Journal of Physics: Condensed Matter*, vol. 29, p. 465901, oct 2017.
- [30] G. Prandini, A. Marrazzo, I. E. Castelli, N. Mounet, and N. Marzari, “Precision and efficiency in solid-state pseudopotential calculations,” *npj Computational Materials*, vol. 4, p. 72, Dec 2018.
- [31] H. J. Monkhorst and J. D. Pack, “Special points for brillouin-zone integrations,” *Phys. Rev. B*, vol. 13, pp. 5188–5192, Jun 1976.
- [32] J. P. Perdew, K. Burke, and M. Ernzerhof, “Generalized gradient approximation made simple,” *Phys. Rev. Lett.*, vol. 77, pp. 3865–3868, Oct 1996.
- [33] G. K. Madsen and D. J. Singh, “Boltztrap. a code for calculating band-structure dependent quantities,” *Computer Physics Communications*, vol. 175, no. 1, pp. 67–71, 2006.
- [34] R. M. Tromer, L. C. Felix, C. F. Woellner, and D. S. Galvao, “A dft investigation of the electronic, optical, and thermoelectric properties of pentadiamond,” *Chemical Physics Letters*, vol. 763, p. 138210, 2021.
- [35] M. Markov, S. E. Rezaei, S. N. Sadeghi, K. Esfarjani, and M. Zebarjadi, “Thermoelectric properties of semimetals,” *Phys. Rev. Mater.*, vol. 3, p. 095401, Sep 2019.
- [36] E. Pakizeh, J. Jalilian, and M. Mohammadi, “Electronic, optical and thermoelectric properties of fe₂zrp compound determined via first-principles calculations,” *RSC Adv.*, vol. 9, pp. 25900–25911, 2019.
- [37] H. Alavi-Rad, A. Kiani-Sarkaleh, S. Rouhi, and A. Ghadimi, “Investigation of the electronic and thermoelectric properties of hydrogenated monolayer germanene under biaxial tensile and compressive strains by dft approach,” *Physica E: Low-dimensional Systems and Nanostructures*, vol. 124, p. 114339, 2020.
- [38] D. Behera, M. Manzoor, and S. K. Mukherjee, “Incorporation of te in enhancing thermoelectric response of aeag₂sete (ae = sr, ba) compounds: A dft insight,” *Computational Condensed Matter*, vol. 33, p. e00757, 2022.
- [39] C.-T. Toh, H. Zhang, J. Lin, A. S. Mayorov, Y.-P. Wang, C. M. Orofeo, D. B. Ferry, H. Andersen, N. Kakenov, Z. Guo, I. H. Abidi, H. Sims, K. Suenaga, S. T. Pantelides, and B. Özyilmaz, “Synthesis and properties of free-standing monolayer amorphous carbon,” *Nature*, vol. 577, pp. 199–203, Jan 2020.